ADVANCED MATERIALS
www.advmat.de

www.MaterialsViews.com

Multiferroic Operation of Dynamic Memory Based on Heterostructured Cantilevers

*Tiberiu-Dan Onuta, Yi Wang, Samuel E. Lofland, and Ichiro Takeuchi**

Multiferroic materials and structures have ushered in new types of electronic devices whose operation mechanisms are based on electric field control of magnetism.[1–3] In addition, heterostructured multiferroics have been previously used to demonstrate ultrahigh sensitivity magnetic field sensors,[4–6] typically consisting of piezoelectric/magnetostrictive multilayers. In such heterostructured devices, elastomechanical properties serve as a medium of multiferroic signal transduction.

Microelectromechanical systems (MEMS) can provide platforms for a variety of multifunctionalities including sensing, actuation,[7,8] energy conversion, storage and harvesting,[9] and spin reorientation transition.[10,11] Here, we have developed miniaturized arrays of multiferroic cantilever devices on a MEMS platform where various energy scales (mechanical, magnetic (Zeeman, anisotropy)) are comparable in magnitude, and the mechanical degree of freedom emerges as a key tunable device parameter that is directly coupled to multiferroic properties. By operating them in the non-linear regime, we show that enhanced mechanical coupling at the tunable resonant frequency results in bistable dynamic states that can be reversibly switched by DC magnetic or electric fields. Our multiferroic memory devices on Si wafers are scalable with high fabrication yields, and have stable read/write operations which have been tested for 10^4 cycles.

We have fabricated heterostructured cantilever arrays on 4″ Si wafers buffered with oxide/nitride/oxide (ONO) multilayers. The initial silicon oxide/nitride/oxide (ONO) stack was deposited on Si (100) wafers by a PE-CVD (plasma enhanced-chemical vapor deposition) process. The ONO stack starts with a 100-nm thick silicon oxide (bottom) layer and contains six layers of 75-nm thick silicon nitride separated by 100-nm thick silicon oxide layers. The last silicon oxide (upper) layer is thicker, only to complete a 3.8-μm thick ONO stack. The ONO stack was used to fine tune the stress in the cantilevers.[12] A Pt/Ti (90 nm/20 nm) bilayer was sputtered at 450 °C. This bilayer also serves as the bottom electrode of the multiferroic device. A 500-nm sol-gel $Pb(Zr_{0.52}Ti_{0.48})O_3$ (PZT) multilayer was deposited and annealed on the device bottom electrode. The magnetostrictive $Fe_{0.7}Ga_{0.3}$ layer was then sputtered at room temperature. The device heterostructure was etched top-down using a four-mask lithographic process including ion milling of $Fe_{0.7}Ga_{0.3}$ and PZT layers, PZT wet etching to uncover the bottom electrode pads and XeF_2-based etching of Si to release the cantilevers.

Strong magnetoelectric (ME) coupling at the FeGa/PZT interface leads to the ME coefficient (a measure of magnetic-field-induced electric field) in the range of 30–50 V Oe^{-1} cm^{-1} (in the CGS units system) at the mechanical resonant frequency f_R of the cantilever in vacuum.[9] The typical value of the quality factor Q at f_R is 2500 in vacuum. The cantilever length L in the present experiment is 1 mm, and the width w and thickness b are 200 μm and 5 μm, respectively. The fabrication yield of successfully released and operational devices is approximately 90% (out of 300 devices/wafer).

The basic operation of our devices consists of driving the cantilever at f_R using AC magnetic field H_{AC} or AC electric field E_{AC} (voltage V_{AC})[13] and applying DC magnetic field H_{DC} and/or DC electric field E_{DC} to induce change in the dynamic state of the cantilever which can be read off by the piezoelectric signal (see Supporting Information).[14] A central feature of our devices is that there is an enhanced multiferroic signal transduction (induced piezoelectric voltage due to strain) at f_R, and f_R can be continuously tuned by H_{DC} and E_{DC}.

The transduced piezoelectric signal S_{ME} as a result of ME coupling at f_R varies as a function of H_{DC}, as seen in an extended butterfly curve (**Figure 1**a), and the dependence of f_R on H_{DC} is separately also plotted in Figure 1b. The magnetic field at which sudden changes in f_R take place on the curve corresponds to the coercive field H_C of the FeGa film, where S_{ME} displays maximum values as a result of enhanced ME susceptibility (Figure 1a). Figure 1a shows that a large ME signal can be attained at zero magnetic field bias ($H_{DC} = 0$). We note that the significant ME signal at zero magnetic field bias is a unique feature of our cantilevers: the lack of this effect in larger sized devices ($L >> 1$ mm, $b >> 5$ μm) requires H_{DC} bias for achieving significant signal transduction.[4,15]

The average total energy of the cantilever is given by $\langle U \rangle = k_{eff}A^2$, where k_{eff} is the effective spring constant of the cantilever, and A is the amplitude of the oscillation. The device total energy consists of two main contributions, namely elastic and magnetic terms:

$$\langle U \rangle = \langle U_{elastic} \rangle + \langle U_{magnetic} \rangle = \frac{wb}{3L}\left(\frac{b^2}{4L^2}\langle Y \rangle + MH_{DC}\frac{b_m}{b} \right) A^2 \qquad (1)$$

where b_m is the magnetic film thickness, M is the magnetization along the beam axis, and $\langle Y \rangle$ is the weighted Young's modulus of the entire cantilever. These two energy terms are

Dr. T.-D. Onuta, Prof. I. Takeuchi
Department of Materials Science and Engineering
University of Maryland
College Park, MD 20742, USA
E-mail: takeuchi@umd.edu
Dr. Y. Wang
Department of Physics
University of Maryland
College Park, MD 20742, USA
Prof. S. E. Lofland
Department of Physics and Astronomy
Rowan University
Glassboro, NJ 08028, USA

DOI: 10.1002/adma.201402974

© 2014 WILEY-VCH Verlag GmbH & Co. KGaA, Weinheim

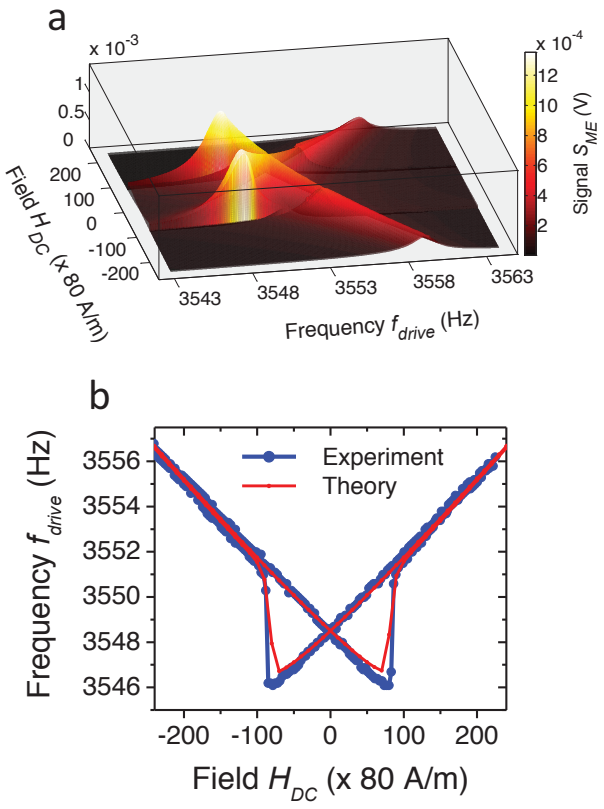

Figure 1. Characteristics of a multiferroic cantilever in linear regime. a) Extended butterfly curve of the multiferroic device. The AC magnetic excitation is H_{AC} = 80 A/m (RMS). The vertical scale is the device signal (also color coded for clarification). b) Hysteretic dependence of f_R on H_{DC} (extracted from Figure 1a). The first flexural mode of the device is at f_{R0} = 3548.7 Hz. Both H_{AC} and H_{DC} were aligned along the cantilever length direction. Measurements were carried out in vacuum of 3.5×10^{-4} mbar. The theory fit $f_{R,magnetic} = f_{R,magnetic}(H_{DC})$ is described in the Supporting Information.

comparable in magnitude in the present device, and thus, they contribute equally to k_{eff}. However, when $b >> b_m$, the elastic energy becomes substantially larger than the magnetic term (in larger-sized devices).

To understand the H_{DC}-dependent f_R of our multiferroic cantilevers, we developed a continuum dynamics model based on a Lagrangian (see Supporting Information). Assuming that the energy in the FeGa film is much smaller than that of the entire cantilever, the Lagrange formalism leads to the Euler–Bernoulli beam equation, from which the expression for the H_{DC}-field dependent resonance frequency, $f_{R,magnetic}$, can be derived as:

$$f_{R,magnetic}(H_{DC}) = f_{R0}\left\{1+\left[\frac{1}{2\pi\rho_{avg}}\left(\frac{b_m}{b}\right)\frac{\gamma}{f_{R0}}\frac{\mu_0 H_{DC} M(H_{DC})^2\left(H_{DC}+\frac{1}{2}M(H_{DC})\right)}{\left(H_{DC}+M(H_{DC})\right)^2}+\frac{3b_m}{2(b-b_m)}\lambda(H_{DC})\frac{\Delta Y_m(H_{DC})}{Y_s}\right]\right\} \quad (2)$$

Here, $\gamma = \zeta^2/f_{R0} = \sqrt{\rho_{avg} wb/(YI)_{avg}}$, where f_{R0} is the natural resonant frequency of the fundamental mode, ζ (= 1.9/L) is the propagation constant for this mode, ρ_{avg} is the weighted density of the entire cantilever, $(YI)_{avg}$ is a weighted average of the product of effective Young's modulus and second moment of inertia of films representing the bending stiffness of the cantilever. μ_0 is the magnetic permeability of free space. The last term in Equation 2 (which is much smaller than the other terms) leads to the resonant frequency shift due to the H_{DC}-dependent Young's modulus Y_m in the magnetic FeGa film, where $\Delta Y_m = Y_m(H_{DC}=0) - Y_m(H_{DC})$. Y_s is the weighted effective Young's modulus of the multi-layered substrate and $\lambda = \lambda(H_{DC})$ is the magnetostriction of FeGa. We note that the main contribution to the device frequency shift is the magnetic torque, not the magnetostriction. When $\frac{b_m}{b} \to 0$ or $\frac{b_m}{b-b_m} \to 0$, we obtain $f_{R,magnetic}(H_{DC}) \to f_{R0}$ (from Equation 2).

Figure 1b shows that there is a good agreement between the experimentally obtained curve and the theoretically obtained expression for $f_{R,magnetic} = f_{R,magnetic}(H_{DC})$. The input data set for the theory fit includes the measured magnetization hysteresis $M = M(H_{DC})$ (see Supporting Information). The developed theory can also be used to understand why the larger scale ME devices do not display H_{DC}-dependent f_R. In the limit when the magnetic film thickness is much smaller than the total thickness or the substrate thickness of the cantilever (which results in strong substrate clamping of the device), $F_{R,magnetic}(H_{DC})$ approaches f_{R0} (the resonant frequency at zero magnetic field bias), which explains the lack of frequency shift in the measured butterfly curves of larger devices.[15]

The modulation of the spring constant in piezoelectric cantilevers due to E_{DC} is known to lead to shifting of the resonant frequency, $f_{R,electric} = f_{R,electric}(E_{DC})$[16] (see Supporting Information). For our multiferroic cantilever devices, application of either DC electric and/or DC magnetic field bias can bring about effective stiffening of the beam; i.e., increase in f_R. Because there are two separate actuation schemes (magnetic and electric) in our devices, we thus can write a combined expression for the resonant frequency of multiferroic cantilevers as:

$$f_{R,multiferroic}(H_{DC},E_{DC}) = (1/f_{R0}) \cdot f_{R,magnetic}(H_{DC}) \cdot f_{R,electric}(E_{DC}) \quad (3)$$

To turn our multiferroic cantilever into a memory device, we need a mechanism to induce and control bistable states.

We exploit the modulation of the amplitude response of a Duffing oscillator,[17] and use its dual-solution state in the nonlinear regime. This can be established in our cantilevers by AC excitation of either $H_{AC} \geq 240$ A/m (RMS) or $E_{AC} \geq 1.2 \times 10^5$ V/m (RMS).[13] In this regime, the device response signal S_{ME} as a function of driving frequency no longer has a Lorentzian shape, and develops a hysteresis behavior: the response now depends on the frequency sweeping direction. When f_{drive} is scanned in the increasing direction, the response peak is a distorted non-Lorentzian, and it is blue-shifted (**Figure 2**, see the upper curve peak in the upper left inset).

The Duffing oscillator has two amplitude solutions (A_1 and A_2) giving rise to the hysteresis in the oscillation amplitude–frequency relation,[17] which can be traced by sweeping the AC

© 2014 WILEY-VCH Verlag GmbH & Co. KGaA, Weinheim

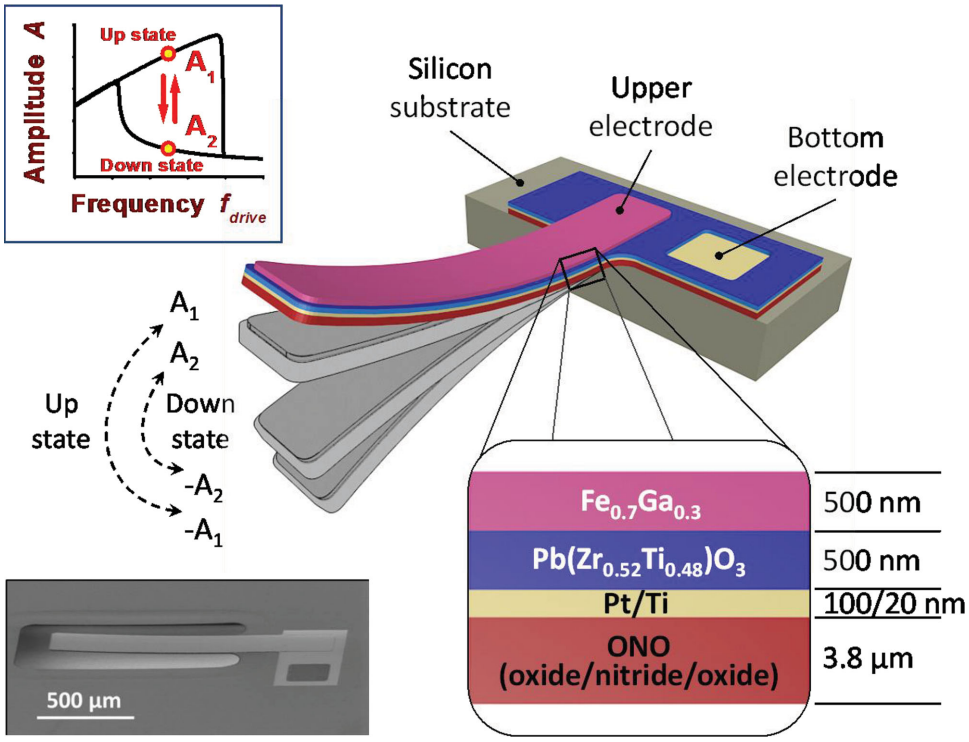

Figure 2. Schematic illustrating mechanical bistable states of the ME device (with a zoomed-in cross-sectional structure of the device). Upper left inset: Hysteretic frequency response of the multiferroic device showing two amplitude states $A_1(f_{drive})$ and $A_2(f_{drive})$ (defining the up and down states, respectively) of the mechanical displacement at a given driving frequency. Lower left inset: an SEM image of a cantilever multiferroic device.

driving frequency f_{drive} in both directions. The two branches of the oscillation amplitude in the hysteresis correspond to two dynamical states (up and down) which can be directly probed by measuring the device signal S_{ME} (Figure 2).

By applying H_{DC} (or E_{DC}), both the Duffing hysteresis envelope and the frequency f_R of the device can be shifted in the S_{ME}–f_{drive} space, and upon taking the field off, the system goes back to the original hysteresis position and f_R.

The translation of the hysteresis region in the frequency space can result in switching the states from up to down or down to up when the shifted hysteresis curve temporarily takes the intermediate state outside of the initial hysteresis envelope (or equivalently, the initial f_R position in the S_{ME}–f_{drive} space remains outside of the shifted hysteresis envelope). Using this principle, we have demonstrated reversible operations of a two-state multiferroic bit memory using input signals in the form of DC magnetic field H_{DC} (**Figure 3**a,b) or a DC voltage V_{DC} (Figure 3c,d). An excitation H_{AC} of 428 A/m (RMS) is first applied along the cantilever to place it in the non-linear regime. In Figure 3a, we show the mechanism of switching between the two states when the DC magnetic field pulses are applied. In addition to the temporary translation of the hysteresis in the frequency space, there is temporary change in the hysteresis width as seen in Figure 3a. With the initial condition of $H_{DC} = 0$ and $V_{DC} = 8.1$ V, the cantilever displays the hysteresis labeled Hyst 1 in the frequency space. The frequency of H_{AC} is selected so that it is inside the hysteresis loop. Figure 3a depicts how the H_{DC} pulse results in the upstate switching to the down state and vice versa. Once the pulse of $H_{DC} = 5.6$ kA/m is applied (Figure 3b), the original f_R is temporarily in the intermediate range outside the envelope of Hyst 2. Upon returning to Hyst 1, the switching has now taken place, and the device is in its up state. To go back to the original state, we apply a DC magnetic field pulse of the same magnitude with an opposite sign: the hysteresis loop now shifts in the opposite direction as Hyst 3, and upon returning, the device is in its original state.

Because the mechanism of temporary shifting of f_R is through induced strain, the state-switching operation can also be accomplished using V_{DC} as the input (Figure 3c,d). We have carried out initial testing of repeating read-write-read-erasure operations up to 10^4 cycles in one device and found no failed operations. We note that due to the fact that strain can be simultaneously induced by magnetostriction and piezoelectricity, it is possible to combine H_{DC} and V_{DC} pulses as additive input for our memory device. Such versatile multiferroic operation modes can open the door to various novel dynamic memory schemes. The present scheme of biferroic memory represents a departure from other types of multiferroic memory previously reported.[18–21]

In conclusion, we have demonstrated multiferroic operation of a dynamic memory using integrated heterostructured cantilevers. It is known that nanoelectromechanical systems (NEMS) can operate at frequencies up to gigahertz.[22–25] Thus, high speed operation of the present device can be realized by going to nanoscale cantilever or doubly-clamped devices. For instance, keeping the same aspect ratio of the cantilever (and keeping also the other dimensional parameters the same), if we decreased the length L of the cantilever to 10 µm, then

© 2014 WILEY-VCH Verlag GmbH & Co. KGaA, Weinheim

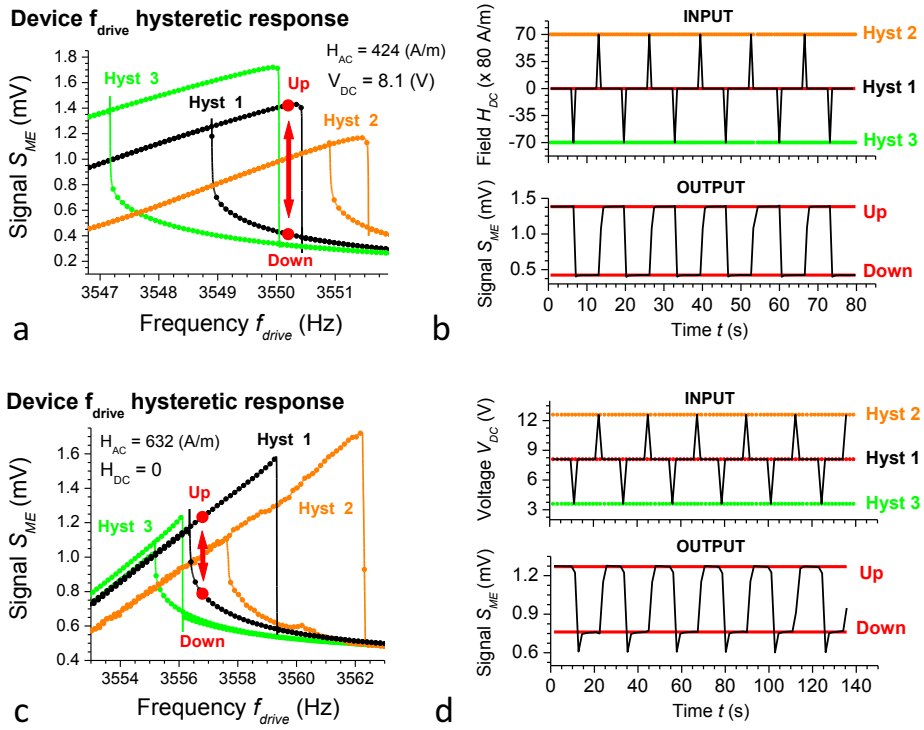

Figure 3. Multiferroic memory device with DC magnetic field bias H_{DC} and DC voltage V_{DC} as input. a) Translation of the hysteresis position with H_{DC} as input. The AC magnetic excitation is H_{AC} of 424 A/m (RMS). b) Output multiferroic device signal when the input is based on $\Delta H_{DC} = \pm 5.6$ kA/m pulses. c) Translation of the hysteresis position with V_{DC} as input (see Supporting Information). In this case, the AC magnetic excitation is H_{AC} of 632 A/m (RMS). d) Output multiferroic device signal when the input is based on $\Delta V_{DC} = \pm 4.5$ V pulses.

f_{R0} (which goes as $1/L^2$) would be ca. 35 MHz. The intrinsic limit of the operation speed of our devices is given by the piezoelectric and magnetic response. The piezo-response time is the time sonic wave takes to traverse through the PZT film. For a 500-nm-thick PZT film, upon application of an electric field pulse, this takes about 100 ps, which corresponds to 10 GHz. Ferromagnetic resonance limits the magnetization rotation speed, and this is about a few gigahertz. Equation 2 shows that even for such a high f_{R0}, the field required to shift the frequency, and thus, the required switching field of the device will be of the same order as measured here.

Non-linear cantilevers and doubly-clamped beams are often driven by external shakers[26] or by electrostatic means.[27–30] In comparison, driving of our heterostructured multiferroic devices is controlled by piezoelectric and/or magnetostrictive actuation. Our newly developed theory of magnetic cantilevers describes the basis for how: i) the occurrence of the resonant frequency change (in linear regime) is determined by the relative thicknesses of the magnetic layer to the bulk thickness of the device, and ii) DC magnetic field can be used to perform the bit operation. An H_{DC}-induced critical point (at a given excitation H_{AC}) in the extended butterfly region separates two distinctive zones of the multiferroic cantilever dynamics (with non-linear/linear regimes) (see Supporting Information). The H_{DC}-bias tunability of the cantilever dynamic response between these two regimes gives control over the width of the hysteresis where the memory is implemented. The switching scheme of our device is such that it can also serve as the basis for the logic devices such as flip-flops and inverters with DC magnetic and electric fields as input.

Supporting Information

Supporting Information is available from the Wiley Online Library or from the author.

Acknowledgements

This work was supported by the DARPA HUMS Program (DARPA DSO FA86500917944) and partially supported by ARO W911NF-07–1–0410 and UMD-NSF MRSEC (DMR 0520471). The authors acknowledge support from the staff at the Maryland Nanocenter Fablab and at the Cornell Nano-Scale Science and Technology Facility (CNF), where the devices were fabricated. We also acknowledge Luz Sanchez and Ron Polcawich for valuable discussions.

Received: July 4, 2014
Revised: August 31, 2014
Published online: October 18, 2014

[1] M. Gajek, M. Bibes, S. Fusil, K. Bouzehouane, J. Fontcuberta, A. Barthélémy, A. Fert, *Nat. Mater.* **2007**, *6*, 296.
[2] S. Wu, S. Cybart, P. Yu, M. Rossell, J. Zhang, R. Ramesh, R. Dynes, *Nat. Mater.* **2010**, *9*, 756.

© 2014 WILEY-VCH Verlag GmbH & Co. KGaA, Weinheim

[3] J. Allibe, S. Fusil, K. Bouzehouane, C. Daumont, D. Sando, E. Jacquet, C. Deranlot, M. Bibes, A. Barthélémy, *Nano Lett.* **2012**, *12*, 1141.
[4] H. Greve, E. Woltermann, H. Quenzer, B. Wagner, E. Quandt, *Appl. Phys. Lett.* **2010**, *96*, 182501–1.
[5] Y. Wang, D. Gray, D. Berry, J. Gao, M. Li, J. Li, D. Viehland, *Adv. Mater.* **2011**, *23*, 4111.
[6] J. Gao, D. Gray, Y. Shen, J. Li, D. Viehland, *Appl. Phys. Lett.* **2011**, *99*, 153502–1.
[7] K. Eom, H. Park, D. Yoon, T. Kwon, *Phys. Rep.* **2011**, *503*, 115.
[8] S. Baek, J. Park, D. Kim, V. Aksyuk, R. Das, S. Bu, D. Felker, J. Lettieri, V. Vaithyanathan, S. Bharadwaja, N. Bassiri-Gharb, Y. Chen, H. Sun, C. Folkman, H. Jang, D. Kreft, S. Streiffer, R. Ramesh, X. Pan, S. Trolier-McKinstry, D. Schlom, M. Rzchowski, R. Blick, C. Eom, *Science* **2011**, *334*, 958.
[9] T. D. Onuta, Y. Wang, C. J. Long, I. Takeuchi, *Appl. Phys. Lett.* **2011**, *99*, 203506–1.
[10] N. Tiercelin, V. Preobrazhensky, P. Pernod, A. Ostaschenko, *Appl. Phys. Lett.* **2008**, *92*, 062904–1.
[11] N. Tiercelin, A. Talbi, V. Preobrazhensky, P. Pernod, V. Mortet, K. Haenen, A. Soltani, *Appl. Phys. Lett.* **2008**, *93*, 161902–1.
[12] J. Pulskamp, A. Wickenden, R. Polcawich, B. Piekarski, M. Dubey, G. Smith, *J. Vac. Sci. Technol. B* **2003**, *21*, 2482.
[13] T. Onuta, Y. Wang, C. Long, S. Lofland, I. Takeuchi, *Appl. Phys. Lett.* **2012**, *101*, 043506–1.
[14] H. Noh, S. B. Shim, M. Jung, Z. G. Khim, J. Kim, *Appl. Phys. Lett.* **2010**, *97*, 033116–1.
[15] P. Zhao, Z. L. Zhao, D. Hunter, R. Suchoski, C. Gao, S. Mathews, M. Wuttig, I. Takeuchi, *Appl. Phys. Lett.* **2009**, *94*, 243507–1.
[16] Q. Wang, T. Zhang, Q. Chen, X. Du, *Sens. Actuators, A* **2003**, *109*, 149.
[17] A. H. Nayfeh, D. T. Mook, *Nonlinear Oscillations*, Wiley-VCH, Weinheim, Germany **1995**, p. 720.
[18] S. Giordano, Y. Dusch, N. Tiercelin, P. Pernod, V. Preobrazhensky, *Phys. Rev. B* **2012**, *85*, 155321–1.
[19] N. Tiercelin, Y. Dusch, A. Klimov, S. Giordano, V. Preobrazhensky, P. Pernod, *Appl. Phys. Lett.* **2011**, *99*, 192507–1
[20] A. Brandlmaier, S. Gepraegs, G. Woltersdorf, R. Gross, S. T. B. Goennenwein, *J. Appl. Phys.* **2011**, *110*, 043913–1.
[21] T. Wu, M. Bao, A. Bur, H. K. D. Kim, K. P. Mohanchandra, C. S. Lynch, G. P. Carman, *Appl. Phys. Lett.* **2011**, *99*, 182903–1.
[22] M. Li, H. Tang, M. Roukes, *Nat. Nanotechnol.* **2007**, *2*, 114.
[23] M. Bagheri, M. Poot, M. Li, W. Pernice, H. Tang, *Nat. Nanotechnol.* **2011**, *6*, 726.
[24] S. Verbridge, H. Craighead, J. Parpia, *Appl. Phys. Lett.* **2008**, *92*, 013112–1.
[25] X. M. H. Huang, C. A. Zorman, M. Mehregany, M. L. Roukes, *Nature* **2003**, *421*, 496.
[26] W. J. Venstra, H. J. R. Westra, H. S. J. van der Zant, *Appl. Phys. Lett.* **2010**, *97*, 193107–1.
[27] I. Kozinsky, H. W. C. Postma, I. Bargatin, M. L. Roukes, *Appl. Phys. Lett.* **2006**, *88*, 253101–1.
[28] D. N. Guerra, M. Imboden, P. Mohanty, *Appl. Phys. Lett.* **2008**, *93*, 033515–1.
[29] R. L. Badzey, G. Zolfagharkhani, A. Gaidarzhy, P. Mohanty, *Appl. Phys. Lett.* **2004**, *85*, 3587.
[30] M. Faucher, B. Grimbert, Y. Cordier, N. Baron, A. Wilk, H. Lahreche, P. Bove, M. Francois, P. Tilmant, T. Gehin, C. Legrand, M. Werquin, L. Buchaillot, C. Gaquiere, D. Theron, *Appl. Phys. Lett.* **2009**, *94*, 233506–1.

© 2014 WILEY-VCH Verlag GmbH & Co. KGaA, Weinheim